Magnetic field effects in terahertz quantum-cascade lasers

INSTITUTE OF PHYSICS PUBLISHING SEMICONDUCTOR SCIENCE AND TECHNOLOGY

Semicond. Sci. Technol. **19** (2004) S348–S350 PII: S0268-1242(04)71946-X

Magnetic field effects in terahertz quantum-cascade lasers

V Tamosiunas[1], R Zobl[1], G Fasching[1], J Ulrich[1], G Strasser[1], K Unterrainer[1], R Colombelli[2], C Gmachl[2], K West[2], L Pfeiffer[2] and F Capasso[3]

[1] Institut für Festkörperelektronik, Technische Universität Wien, Floragasse 7, A-1040 Vienna, Austria

[2] Bell-Laboratories, Lucent Technologies, 600 Mountain Ave, Murray Hill, NJ 07974, USA

[3] Division of Engineering and Applied Sciences, Harvard University, Pierce Hall, 29 Oxford St, Cambridge, MA 02138, USA

E-mail: Vincas@fkeserver.fke.tuwien.ac.at

Received 28 July 2003
Published 10 March 2004
Online at stacks.iop.org/SST/19/S348 (DOI: 10.1088/0268-1242/19/4/115)

Abstract

We have measured the emission intensity and spectra of terahertz quantum-cascade lasers in an external magnetic field applied normal to the epilayers. We have observed a reduction of the threshold current, an enhancement of laser emission intensity and shifts of the emission line. A wider operating range was predicted for the selected waveguide design according to our finite-difference time-domain simulation results. The intensity enhancement and the threshold current reduction are attributed to the suppression of nonradiative Auger-intersubband transitions by Landau quantization of the in-plane electron motion, to the modulation of the injection rate via resonant inter-Landau-level transfer, and to the modulation of waveguide properties.

The first quantum cascade laser (QCL) in the terahertz range was recently demonstrated by Köhler *et al* [1] proving that QCL concept can be successfully implemented also in far-infrared region. The continuous wave operation of the THz QCL was also reported [2]. However, the further improvement of THz QCLs and lasing at even longer wavelengths is a challenge for different reasons related to the intersubband population dynamics and the waveguide properties. Electron–electron scattering and interface roughness are the main scattering mechanisms at low temperatures in this range of intersubband energies. They lead to fast carrier relaxation, counteracting population inversion.

An external magnetic field applied normal to epilayers should lead to an additional quantization of the in-plane electron motion [3] and to the modification of the scattering. The recently observed enhancement of the luminescence intensity of GaAs/AlGaAs [4] and InGaAs/InAlAs [5] terahertz quantum cascade structures confirms such an effect. Strong oscillations of the mid-IR QCL emission intensity as a function of the magnetic field were also recently reported [6].

The system used in the emission experiments consists of a FTIR spectrometer (NICOLET Magna IR 850) equipped with a Si-beamsplitter and a 4.2 K Si-bolometer. For the magnetic field measurements, the THz QCL is mounted in a magnet cryostat with two superconducting magnets. In this cryostat, detection is possible by a magnetic field tunable InSb cyclotron resonance detector, by a broadband Ga doped Ge detector, or by the external FTIR (figure 1).

The magnetic field at the location of the sample (oriented perpendicular to the epitaxial layers) can be adjusted independently from 0 T to 6.7 T by a second magnet. A closed light pipe guides the radiation from the sample to the detector. This narrow band InSb detector [4] is tuned by the magnetic field of the second (detector) superconducting magnet. The whole spectrometer is immersed in liquid He, so that room temperature background radiation cannot distort the measurements.

A 4.5 THz quantum-cascade laser, based on the active structure design proposed in [1], was used for the measurements in a magnetic field. 100 periods of the active structure were sandwiched between two n^+-doped contact layers (the bottom layer was $d = 500$ nm thick with $n = 4 \times 10^{18}$ cm^{-3} doping, the top layer was $d = 100$ nm thick with

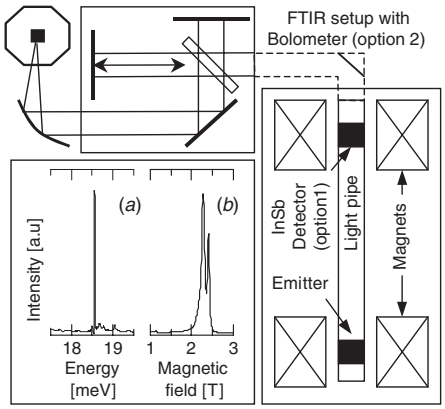

Figure 1. Set-up for high resolution spectral measurements: cryostat with superconducting magnets, high resolution (0.0155 meV) Fourier spectrometer and Si-bolometer. (*a*) High-resolution spectrum of the laser without applied magnetic field at the emitter sample. (*b*) Response of the InSb detector versus applied detector magnetic field when illuminated by the THz laser (one line corresponds to the free electron cyclotron resonance, the other one to the impurity bound resonance).

$n = 7 \times 10^{18}$ cm^{-3} doping) grown on a semi-insulating GaAs substrate using molecular beam epitaxy (MBE).

The laser devices were processed as ridges of lateral dimensions of 100, 130 and 200 μm by reactive ion etching through the active zone down to the bottom contact layer. Metallic contacts (15 nm/30 nm/14 nm/200 nm of Ge/Au/Ni/Au) were evaporated for the bottom contact layer with approximately 10 μm separation from the ridge. Two 10 μm wide contact stripes of the same composition were evaporated on top of the ridge with 5 μm separation from the side walls. The sample was annealed for 1 min at 430 °C to alloy the Ohmic contacts. Afterwards, 10 nm/400 nm Ti/Au layers were sputtered on top of the ridge to finish the top contact and to provide waveguiding. The sample was cleaved into 3 mm long devices, soldered with indium onto a copper holder and wire bonded.

A careful selection of doping and thickness for the bottom n^+ layer is essential, since the mode confinement and losses in the case of this QCL design are strongly dependent on the dielectric constant of the n^+ layer [1]. We have performed a series of FDTD simulations to predict the performance of different waveguide designs in a magnetic field. A standard FDTD algorithm [7, 8] was modified to include the finite-difference scheme for solving Maxwell–Bloch equations in a two energy level medium based on the scheme suggested by Ziolkowski *et al* [9] and a finite-difference algorithm based on the Drude–Lorentz model for simulating the performance of the n^+ layer. Simulation results for fixed gain medium parameters and two possible waveguide designs are presented in figure 2. It is clearly seen that while slightly higher losses are expected for a 500 nm thick 4×10^{18} cm^{-3} doped n^+ layer at 0 T when compared to the original design suggested in [1], a broader operation range is expected in a magnetic field.

A 100 μm wide device was selected for the intensity measurements in a magnetic field due to its broadest lasing range. The broadband Ge detector was used to obtain the laser intensity as a function of different sample magnetic fields which is presented in figure 3. The laser emission intensity

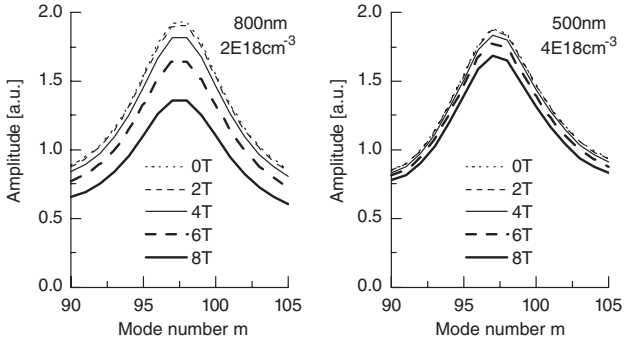

Figure 2. Maximum amplitude versus resonator mode number simulation results for two different n^+ layers.

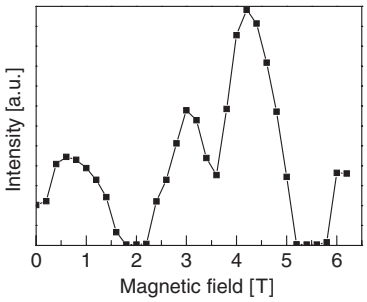

Figure 3. Maximal laser emission intensity versus magnetic field. Laser emission intensity was recorded for every given magnetic field flux density value by adjusting pulse generator settings to obtain the maximum intensity. Clear emission intensity maxima are observed for $N = 2.5$ (4.2 T) and $N = 3.5$ (3 T).

increases substantially for certain values of the magnetic field when compared to $B = 0$ T. For increasing magnetic fields we observe oscillations with a larger period. The application of a magnetic field increases the laser intensity by a factor of more than five at $B = 4.2$ T (see figure 3). This effect is understood as a consequence of the discretization of the energy spectrum. In the parabolic dispersion relation in the absence of a magnetic field the energy conservation requirement for intersubband Auger-scattering processes is fulfilled for a continuum of energy changes ΔE (meaning one electron suffers an energy change of $+\Delta E$, the other one a change of $-\Delta E$). However, for a non-vanishing magnetic field the only allowed energy changes ΔE are multiples of the cyclotron resonance energy $\hbar\omega_c$. Since the Auger-scattering rate scales inversely with the associated change in energy and momentum, it is more and more suppressed with increasing Landau-level splitting. The laser intensity is proportional to the inversion which is directly proportional to the injection rate and inversely proportional to the non-radiative relaxation rate.

We first assume that the injection rate is not influenced by the magnetic field. We would expect an oscillatory increase of the laser emission with minima where the magneto-intersubband resonance condition is met:

$$E_2 - E_1 = \frac{\hbar e B_N}{m^*} N.$$

Here $E_2 - E_1$ is the energy difference between the lowest Landau levels of the upper and lower laser transitions, $\hbar$ the Planck constant, e the elementary charge, B_N the magnetic flux density, m^* the effective mass, N is an integer. Resonant

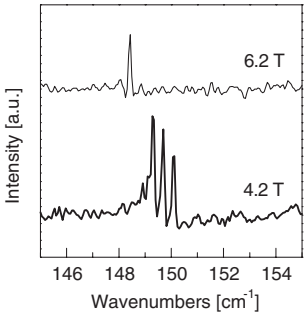

Figure 4. The emission spectra of the 130 μm wide device for two different magnetic field flux density values under constant current conditions.

tunnelling between Landau levels opens up an additional non-radiative relaxation channel via the Landau ladder ($|1, N\rangle, |1, N-1\rangle, \ldots, |1, 0\rangle$) and by reducing the population inversion leads to a decrease in the laser emission intensity. It should be pointed out that a theoretical model proposed by Raikh and Shahbazyan [10] well describes momentum transfer caused by interface roughness or impurities, which is required for resonant transfer between Landau levels of different subbands. It is clearly seen from the figure that the laser stops working at these magneto-intersubband resonances.

The energy difference between the injector states is small ($\sim$3.1–3.8 meV [11]) and the condition for complete magnetic quantization

$$\frac{\hbar eB}{m^*} > \Delta E_{\text{injector}}$$

is reached at relatively low magnetic fields. Optimum performance of the laser should be achieved for $\frac{\hbar eB}{m^*}M = \Delta E_{\text{injector}}$ and $\frac{\hbar eB}{m^*}N \neq \Delta E_{\text{laser}}$, where N and M are integers. The interplay between increased injector efficiency and reduced non-radiative relaxation determines the detailed dependence of the laser intensity on the magnetic field.

The laser intensity increase and oscillatory behaviour was consistently observed for all lasing devices independently of device width. In addition to the increased intensity we observe also a shift of the laser wavelength in the magnetic field. A red shift of laser emission spectra (figure 4) was consistently recorded for all lasing devices made from the described material. A conventional Stark shift can also be observed in this type of structure [12]. However, the observed red shift represents a much 'stronger' effect than Stark shift and therefore differences in level population are the most probable reason for the shift.

In summary, we have observed a reduction of the threshold current, an enhancement of laser emission intensity and shifts of the emission line in an external magnetic field applied normal to epilayers. The operating range of the selected waveguide design is consistent with our finite-difference time-domain simulation results. The intensity enhancement and the threshold current reduction are attributed to the suppression of nonradiative Auger-intersubband transitions by Landau-quantization of the in-plane electron motion, to the modulation of the injection rate via resonant inter-Landau-level transfer and to the modulation of waveguide properties.

Acknowledgments

We acknowledge support by the Austrian Science Foundation (START, ADLIS SFB) and the European Community IST program (Teravision, Supersmile).

References

[1] Köhler R, Tredicucci A, Beltram F, Beere H E, Linfield E H, Davies A G, Ritchie D A, Iotti R C and Rossi F 2002 *Nature* **417** 156
[2] Ajili L, Scalari G, Hofstetter D, Beck M, Faist J, Beere H, Davis G, Linfield E and Ritchie D 2002 *Electron. Lett.* **38** 1675
[3] Blank A and Feng S 1993 *J. Appl. Phys.* **74** 4795
[4] Ulrich J, Zobl R, Unterrainer K, Strasser G and Gornik E 2000 *Appl. Phys. Lett.* **76** 19
[5] Blaser S, Rochat M, Beck M, Hofstetter D and Faist J 2002 *Appl. Phys. Lett.* **81** 67
[6] Becker C, Sirtori C, Drachenko O, Rylkov V, Smirnov D and Leotin J 2002 *Appl. Phys. Lett.* **81** 2941
[7] Yee K S 1966 *IEEE Trans. Antennas Propagat.* **14** 302–7
[8] Taflove A 1995 *Computational Electrodynamics: The Finite-Difference Time-Domain Method* (Norwood, MA: Artech House)
[9] Ziolkowski R W, Arnold J M and Gogny D M 1995 *Phys. Rev.* A **52** 3082–94
[10] Raikh M E and Shahbazyan T V 1994 *Phys. Rev.* B **49** 5531
[11] Köhler R, Iotti R C, Tredicucci A and Rossi F 2001 *Appl. Phys. Lett.* **79** 3920
[12] Tamosiunas V, Zobl R, Ulrich J, Unterrainer K, Colombelli R, Gmachl C, West K, Pfeiffer L and Capasso F 2003 *Appl. Phys. Lett.* **83** 3873